

Effect of local distortions on magnetic and magnetoelectric properties of paramagnetic $\text{Pr}_3\text{Ga}_5\text{SiO}_{14}$ langasite

A. Tikhanovskii ^{1,*}, V. Yu. Ivanov,¹ A. Kuzmenko,¹ E. Constable ², A. Pimenov ² and A. Mukhin ¹

¹*Prokhorov General Physics Institute of the Russian Academy of Sciences, Vavilova 38, 119991 Moscow, Russia*

²*Institute of Solid State Physics, Vienna University of Technology, 1040 Vienna, Austria*



(Received 2 April 2024; accepted 12 June 2024; published 8 July 2024)

Magnetic-field-induced electric polarization has been observed in trigonal noncentrosymmetric paramagnetic $\text{Pr}_3\text{Ga}_5\text{SiO}_{14}$ langasite. We detected quadratic electric polarization along the a axis in the basal ab plane for various magnetic field orientations. Electric polarization along the c axis is only evident starting from the fourth power of magnetic field, in accordance with the trigonal symmetry. The magnetic properties of $\text{Pr}_3\text{Ga}_5\text{SiO}_{14}$ primarily stem from the local anisotropic magnetic moment of the two lowest Pr^{3+} singlets (quasidoublet) in the crystal electric field. The random distribution of Ga/Si in the $2d$ positions leads to a local distortion of the C_2 symmetry and to a distribution of the quasidoublet splitting. By considering the interactions of local moments among different Pr^{3+} positions within a phenomenological approach for the allowed magnetoelectric coupling, we derive the electric polarization in terms of symmetry-allowed combinations of local magnetic susceptibilities and field components. The magnetic field dependence of electric polarization in the basal plane, $P_{a,b*}$, is mainly determined by the accumulation of effective local susceptibilities, exhibiting similar behavior in low fields, while polarization along the c axis, P_c , arises from the nonequivalence of local effective magnetic susceptibilities in different Pr^{3+} positions. Our findings suggest that the temperature dependencies of magnetic and magnetoelectric susceptibilities are highly sensitive to the distribution of the quasidoublet splitting, which reflects the local symmetry breaking.

DOI: [10.1103/PhysRevB.110.014409](https://doi.org/10.1103/PhysRevB.110.014409)

I. INTRODUCTION

The magnetoelectric effect, discovered over half a century ago [1], continues to be a subject of significant interest [2,3]. This interest is not only rooted in fundamental research but also stems from the potential applications of magnetoelectric materials. For instance, integrating such materials into computer memory components [4–7], where magnetic properties can be controlled by an electric field, holds promise for substantial energy savings [8]. However, the interaction between magnetic and electric subsystems often proves to be weak [9], and materials exhibiting this interaction are relatively rare. Consequently, the quest for new materials with strongly interacting magnetic and electric subsystems, coupled with investigations into the physics of the magnetoelectric effect, remains a pressing challenge [10–13].

In this context, the langasite compounds ($\text{La}_3\text{Ga}_5\text{SiO}_{14}$) (LGS) have garnered attention in recent years. They possess a noncentrosymmetric space group $P321$ and can exhibit magnetoelectric properties when magnetic ions are incorporated within the lattice. For example, iron-containing langasites, such as $\text{Ba}_3\text{NbFe}_3\text{Si}_2\text{O}_{14}$, undergo antiferromagnetic ordering at $T_N \approx 27$ K, forming a triangular spiral structure with double magnetic chirality [14,15], and display magnetoelectric properties in external magnetic fields [16–18,20]. On the other hand, the complexity of these magnetic structures can com-

plicate the investigation of the underlying magnetoelectric mechanisms.

In rare-earth langasites $R_3\text{Ga}_5\text{SiO}_{14}$ ($R = \text{Nd}, \text{Pr}, \dots$), studying the microscopic mechanisms of the magnetoelectric effect is more straightforward, as they remain paramagnetic even at very low temperatures down to 30 mK [19,21,22]. This is partially due to a frustration of exchange interactions in a crystal with a kagomelike lattice. The magnetic properties of concentrated rare-earth langasites have been extensively investigated [19,21–26]. $\text{Pr}_3\text{Ga}_5\text{SiO}_{14}$ (PGS) has received special attention due to efforts to identify a spin-liquid state [25], although such a state has not been confirmed [26].

Despite the detailed investigation of magnetic properties in concentrated rare-earth langasites, magnetoelectric properties have only been observed in $\text{Nd}_3\text{Ga}_5\text{SiO}_{14}$ (NGS) [27]. The emergence of the electric polarization could be explained considering the symmetry-allowed magnetoelectric coupling in the spin Hamiltonian of the Nd^{3+} Kramers ion. In addition to NGS, the magnetoelectric effect has been studied in $(\text{La}_{0.985}\text{Ho}_{0.015})_3\text{Ga}_5\text{SiO}_{14}$ langasite (HoLGS) doped with non-Kramer ions Ho^{3+} [28]. The quasidoublet ground state of the Ho^{3+} ion in the crystal field determines the macroscopic magnetic and magnetoelectric properties of HoLGS. Similar to ferro- and alumoborates [29–35] with a related space group $R32$, the ground state of the rare-earth ion plays a crucial role in the behavior of the magnetic and magnetoelectric properties of rare-earth langasites [27,28].

Praseodymium (Pr^{3+}) is a non-Kramers rare-earth ion, like Ho^{3+} . However, in PGS, Pr^{3+} substitutes every lanthanum

*Contact author: tikhanovskii@phystech.edu

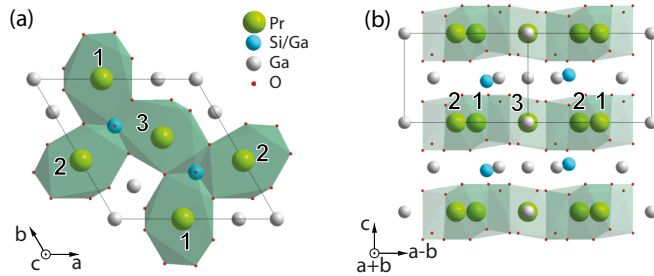


FIG. 1. Crystal structure of PGS langasite seen (a) along the c axis and (b) along the $a + b$ direction. Various ions in different sites are indicated by color spheres. Pr^{3+} ions in magnetically nonequivalent sites are denoted by numbers, 1, 2, and 3. Thin black lines indicate the unit cell with lattice parameters $a = 8.0661 \text{ \AA}$, $c = 5.0620 \text{ \AA}$ [36]. Random occupation of $2d$ sites by Ga or Si ions distorts the local C_2 symmetry of the $3e$ positions for neighboring Pr^{3+} ions.

ion, resulting in a stronger manifestation of magnetoelectric properties (see Fig. 1). The fundamental difference between PGS and HoLGS is in the significantly larger crystal field splitting between the two lowest singlets of the Pr^{3+} , of $\approx 18 \text{ K}$ [26], compared to $\approx 3 \text{ K}$ for Ho^{3+} [28]. The occupation of Ga and Si in the same positions in the local environment of the rare-earth ion breaks the local C_2 symmetry and leads to a distribution of crystal field splittings. Similar to HoLGS, the crystal field splits the Pr^{3+} multiplet and defines the notable distance between the two lowest energy levels (quasidoublet) from the excited states, resulting in significant magnetic anisotropy of the Pr^{3+} ion. Moreover, the observation of a superlattice in LGS [37,38] could result in the existence of more favorable configurations (positions of Ga and Si) and the emergence of more preferable directions of the easy magnetization axis of Pr^{3+} .

This work presents a detailed investigation of magnetic properties of PGS and the first observation of the magnetoelectric effect in it. We experimentally studied the magnetization with magnetic fields directed along the principal crystallographic axes (a , b^* , and c), as well as the magnetic anisotropy in the ab , ac , and b^*c planes. It will be demonstrated that the local environment, with broken symmetry due to the equally probable occupation of Ga and Si ions at the $2d$ sites, determines the ground state of the Pr^{3+} ions. We found that the local magnetic susceptibilities of Pr^{3+} ions determine the macroscopic electric polarization.

II. METHODS

The PGS crystal was grown by Balbashov and Egorov [39] using the floating-zone method. We determined the quality of the crystals by x-ray analysis and by scanning electron microscopy in the z -contrast mode. In both samples, only the langasite phase was detected. The magnetic properties of the langasite samples were studied using a Magnetic Property Measurement System (MPMS-50) by Quantum Design in magnetic fields up to 5 T and at temperatures from 1.9 to 300 K. The pyroelectric studies were performed using a Keithley 6517A electrometer in static fields up to 5 T within the

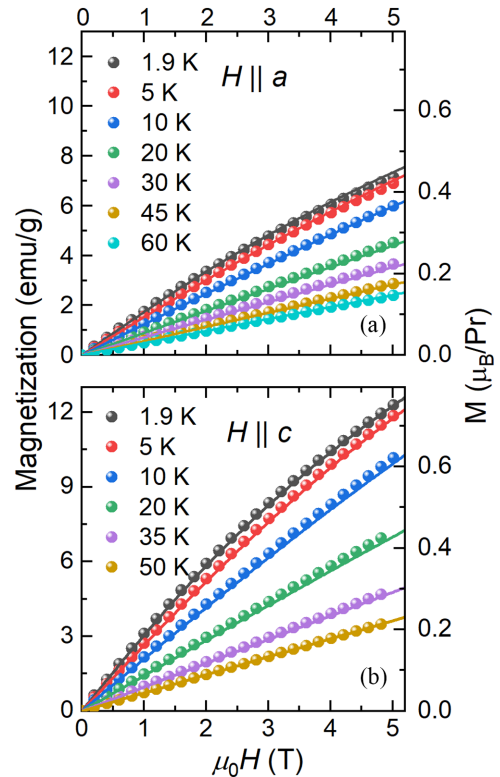


FIG. 2. Field dependencies of the magnetization of PGS for temperatures from 1.9 to 60 K and (a) for $H \parallel a$ and (b) for $H \parallel c$. Open symbols represent experimental data; solid lines correspond to the theory.

MPMS-50 using the original insert. The sample orientation accuracy was around 2° – 5° .

III. EXPERIMENT

A. Magnetic properties

We performed a comprehensive investigation of the magnetic and magnetoelectric properties of PGS including various geometries of measurements. Angular dependencies of the magnetization were measured in the ab^* , b^*c , and ac planes. Additionally, we examined the field dependencies of the magnetization along the principal crystallographic directions at various temperatures as well as the temperature dependencies of the magnetic susceptibility along and perpendicular to the trigonal axis over a wide temperature range.

The magnetization behavior is qualitatively similar for different field orientations. Below 10 K, it displays a nonlinearity without saturation up to 5 T (Fig. 2). Strong anisotropy is evident when the field is oriented in the basal plane ($H \parallel a$, b^*) and perpendicular to it ($H \parallel c$). At $T = 1.85 \text{ K}$ and $\mu_0 H = 5 \text{ T}$ the angular dependence in the ac and bc planes reveals a 180° anisotropy with maxima along the c axis. Additionally, a weak 60° anisotropy in the ab plane [Fig. 3(a)] with maxima along the b^* axis was observed. These angular dependencies correspond to the expected trigonal symmetry. The observed properties are attributed to the crystal field splitting of the Pr^{3+} ground state, specifically resulting in anisotropy of the magnetic moments (see Sec. IV, Theory).

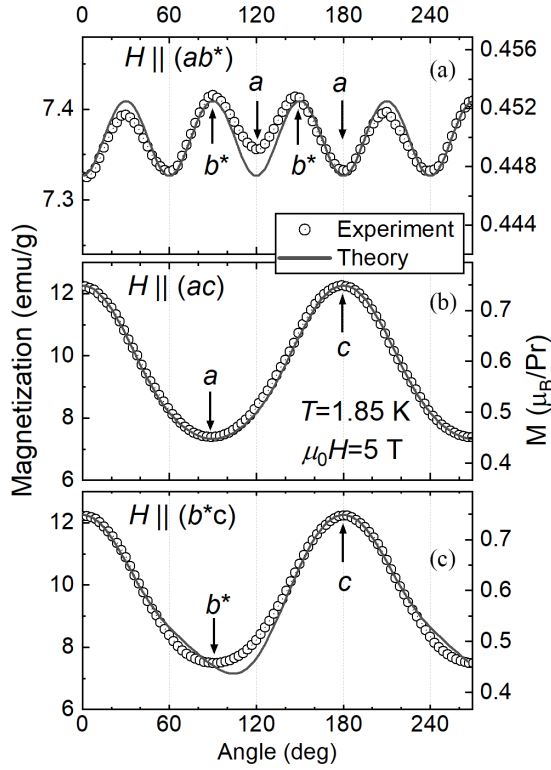


FIG. 3. Angular dependencies of magnetization of PGS in (a) ab^* , (b) ac , and (c) b^*c planes at $T = 1.85 \text{ K}$ in external magnetic field of $\mu_0 H = 5 \text{ T}$. Here, the angle φ_H or θ_H denote rotations of the magnetic field $H = H(\cos \varphi_H \sin \theta_H, \sin \varphi_H \sin \theta_H, \cos \theta_H)$ in the ab^* ($\theta_H = \pi/2$), ac ($\varphi_H = 0$), and b^*c ($\varphi_H = \pi/2$) planes, respectively. Open symbols represent the experimental data; solid lines are theoretical fits with parameters given in Table I.

We measured the temperature dependencies of the magnetic susceptibilities in fields parallel (χ_{\parallel}) and perpendicular (χ_{\perp}) to the trigonal c axis, over a temperature range from 1.9 to 300 K and in the magnetic field of $\mu_0 H = 0.1 \text{ T}$ (Fig. 4). Since below 300 K not all energy levels of the Pr^{3+} multiplet 3H_4 are populated, the magnetic susceptibility cannot be described by the usual Curie-Weiss law [19]. The susceptibilities χ_{\parallel} and χ_{\perp} intersect at $T \approx 160 \text{ K}$ (Fig. 4). At low temperatures ($T \approx 2 \text{ K}$), the susceptibility shows the tendency to saturate at a finite value.

B. Magnetolectric properties

We measured the field-induced electric polarization in PGS up to $\mu_0 H = 5 \text{ T}$ and at temperatures from 1.9 to 160 K. The measurements were conducted in the following geometries: $P_a(H_a)$, $P_a(H_{b^*})$ [Fig. 5(a)], $P_a(H_{a45b45^\circ c})$, and $P_a(H_{a45b135^\circ c})$ [Fig. 5(b)]. In the two latter configurations [Fig. 5(b)], the field is rotated from the c axis in the vertical plane by angles of 45° and 135° , respectively. The rotation plane intersects the ab^* plane at an angle of 45° to the a axis. For the polarization along the c axis, the magnetic field H is rotated by 60° from the c axis in the ac plane [Fig. 5(d)].

The electric polarization depends quadratically on the field with slight deviations at low temperatures and high

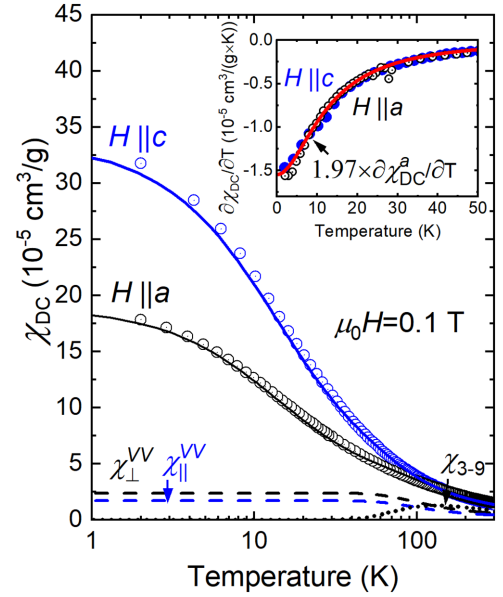


FIG. 4. Temperature dependencies of the magnetic susceptibility of PGS in an external field of $\mu_0 H = 0.1 \text{ T}$, oriented parallel ($H \parallel a$, black) and perpendicular ($H \parallel c$, blue) to the basal plane. Open symbols represent experimental data, while solid lines represent theory. Additionally, the Van Vleck contribution ($\hat{\chi}^{\text{VV}}$) and the contributions from excited levels (χ_{3-9}) to the susceptibility are shown. The inset displays the temperature dependencies of the derivative of the magnetic susceptibility $\partial \chi_{\text{DC}} / \partial T$, demonstrating the same contributions from the two lowest singlets for fields along the a and c axes; the red line represents the derivative of Eq. (10) for $H \parallel c$ ($\partial \chi_{\text{DC}}^a / \partial T$ is scaled by the factor 1.97).

fields [Figs. 5(a) and 5(b)]. Similar to rare-earth ferro- and aluminoborates [29–35], which also possess trigonal symmetry, the quadric (with respect to H) magnetolectric susceptibilities $\alpha_{1,2}^{(2)}(T) \equiv \alpha_{1,2}(T)$ determine the components of the electric polarization in the ab^* plane in quadratic approximation with the magnetic field: $P_a \approx \alpha_1 H_{b^*} H_c + \alpha_2 (H_a^2 - H_{b^*}^2)$ and $P_{b^*} \approx -\alpha_1 H_a H_c - 2\alpha_2 H_a H_{b^*}$.

From the field dependencies of the polarization P_a , we confirmed the expected relations $P_a(H_a) = -P_a(H_{b^*})$ and $P_a(H_{a45b45^\circ c}) = -P_a(H_{a45b135^\circ c})$ within the temperature and field range investigated and determined the quadratic magnetolectric susceptibilities $\alpha_{1,2}$ [Fig. 5(c)] that decrease rapidly with temperature. However, they remain finite in the high-temperature regime. Below $T = 50 \text{ K}$, the temperature dependence of the magnetolectric susceptibilities, like the magnetic ones, is determined by the magnitude and dispersion of the splitting of the two lowest singlets (see Sec. IV, Theory).

Measurements of P_c were conducted in a magnetic field rotated in the ac plane by 60° from the c axis [inset in Fig. 5(d)]. The lowest power in the magnetic field for the induced P_c is four, and the corresponding term is expressed as $\alpha^{(4)}(T) H_a H_c (H_a^2 - 3H_{b^*}^2)$. In the ac plane, it reaches a maximum for the field oriented at 60° to the c axis (geometry $H \parallel a60^\circ c$). In a weak magnetic field ($\mu_0 H < 1 \text{ T}$) or at temperatures above 15 K, the polarization P_c varies approximately as $H^4 T^{-3}$. As the field increases and the temperature

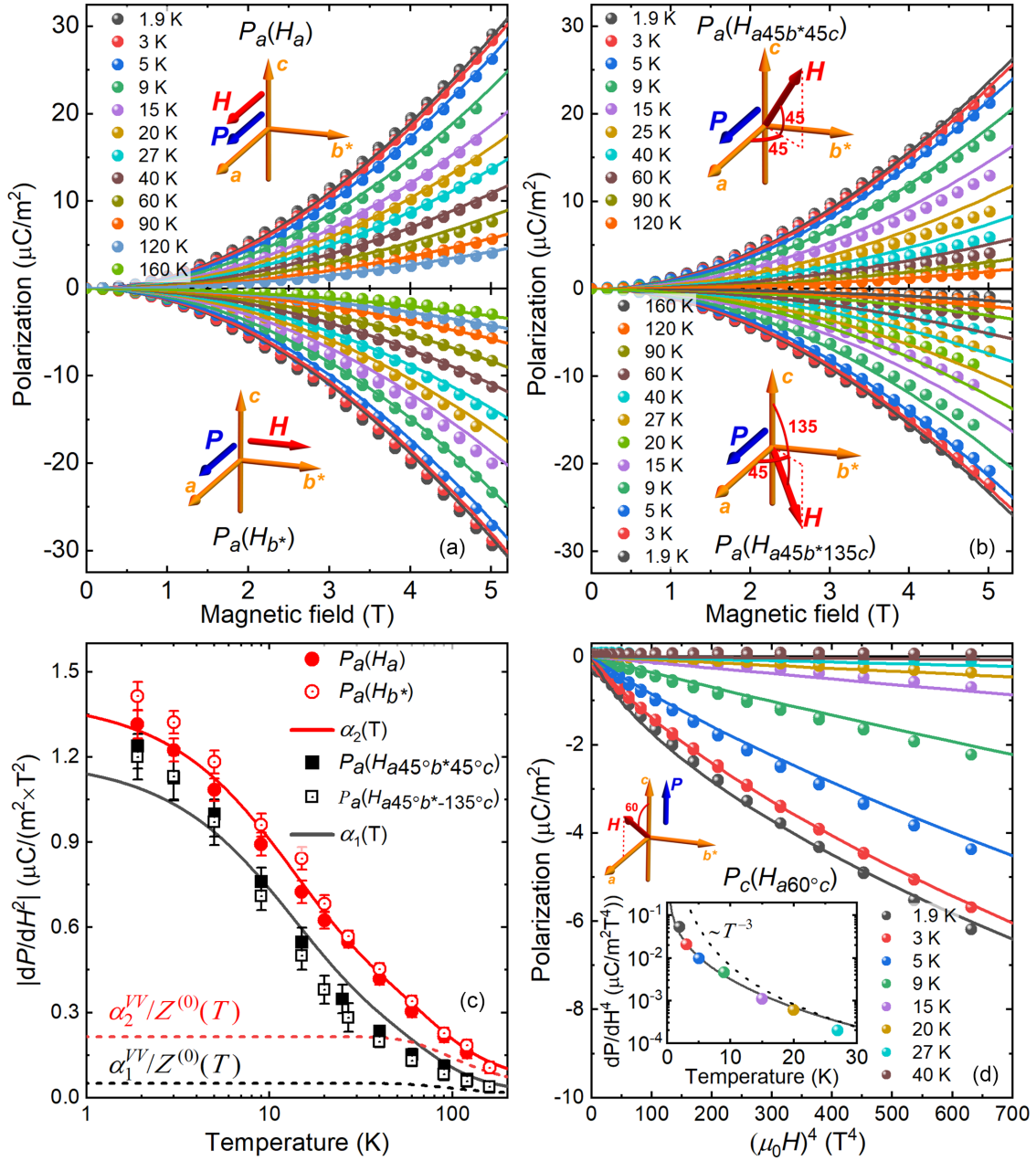


FIG. 5. Field dependencies of the electric polarization P_a in PGS for (a) $H \parallel a, b^*$ and (b) $H \parallel a45^\circ b45^\circ c, a45^\circ b135^\circ c$ at various temperatures. The field is rotated from the c axis in the vertical plane by the angles of 45° and 135° , respectively; the rotation plane intersects the ab^* plane at the angle of 45° to the a axis. (c) Temperature dependencies of the magnetolectric susceptibilities $\alpha_{1,2}(T)$ obtained from the field dependencies of P_a for $H \parallel a, b^*, a45^\circ b^* \pm 45^\circ c$. (d) Dependencies of the electric polarization P_c on the biquadratic field $(\mu_0 H)^4$ at different temperatures. The magnetic field is rotated in the ac plane by 60° from the c axis. The inset shows the temperature dependence of dP/dH^4 , demonstrating the deviation from the behavior $\alpha^{(4)}(T) \sim T^{-3}$ at low temperatures. Symbols represent experimental data; solid lines are theoretical fits with parameters given in Table I.

decreases, the field dependence of the polarization deviates from the H^4 dependence, similar to P_c in $(\text{La}_{1-x}\text{Ho}_x)_3\text{Ga}_5\text{SiO}_{14}$ ($x \approx 0.015$) [28]. The magnetic moments of Pr^{3+} ions remain unsaturated in the field range investigated. However, the deviation from the $P_c \sim H^4$ behavior and the transition to the quasilinear dependence indicate a tendency towards saturation in stronger magnetic fields. At low temperatures, we also observed a deviation of the magnetolectric susceptibility $\alpha^{(4)}(T)$ from the T^{-3} dependence, which was not observed in HoLGS [28].

IV. THEORY

A. The ground state

In PGS, the Pr^{3+} magnetic ions occupy the three C_2 low-symmetry positions, where each local axis coincides with one of the three second-order crystallographic axes ($a, b, -a-b$). The Pr^{3+} ions remain paramagnetic down to low temperatures. The random distribution of Ga and Si in the $2d$ positions leads to a distortion of the local crystal field, breaking the original C_2 symmetry.

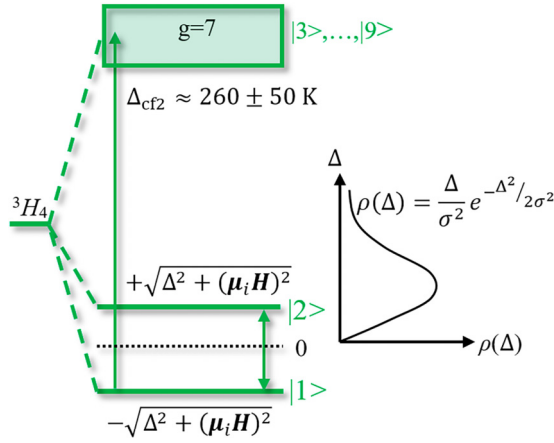


FIG. 6. Schematic representation of the $2J \pm 1 = 9$ energy levels of the Pr^{3+} ion ground multiplet 3H_4 in PGS in the crystal magnetic field. On the right, the Rayleigh function is shown that models the splitting distribution of the two lowest singlets due to random local distortions.

The crystal field V_{cf} of arbitrary $\hat{\chi}$ symmetry (C_1) splits the ground multiplet 3H_4 of the non-Kramers Pr^{3+} ion into $2J + 1 = 9$ singlets. At low temperatures, the two lowest energy levels (a quasidoublet), with a splitting value of Δ , mainly determine the magnetic properties of the rare-earth ion. Random distortions of the crystal field lead to spatial variation of Δ , which we characterize by the Rayleigh distribution (Fig. 6):

$$\rho(\Delta) = \frac{\Delta}{\sigma^2} e^{-\Delta^2/2\sigma^2}. \quad (1)$$

Equation (1) possesses only one parameter σ with a mean value $\bar{\Delta}_{cf} = \sigma\sqrt{\pi/2}$ and a variance $D_{\bar{\Delta}} = \sigma\sqrt{2-\pi/2}$. In reality, the splitting distribution may differ from this simple form; for example, the Voigt distribution is mentioned in Ref. [26]. Determining the distribution function may require additional experiments or complex mathematical calculations; here we employ the simplest distribution that still adequately describes the experimental data (see below).

B. Magnetization

To describe the magnetic properties of PGS and to account for the effect of an external magnetic field \mathbf{H} on the Pr^{3+} rare-earth ion, we use the perturbation theory with the Zeeman term $\hat{V} = \mu_B g_L \hat{\mathbf{J}}\mathbf{H}$ similar to the approach in Ref. [28]. Here, μ_B and $g_L = 4/5$ are the Bohr magneton and the Landé factor, respectively. By projecting the Hamiltonian $\hat{H} = \hat{V}_{cf} + \hat{V}$ onto the subspace of the two lowest singlets of Pr^{3+} , we obtain the 2×2 matrix \hat{H} (within the second-order perturbation theory with respect to \hat{V}):

$$\langle l|\hat{H}|m\rangle = \frac{1}{2}(-1)^l E_{lm} + \langle l|\hat{V}|m\rangle - \sum_{k \neq 1,2} \frac{\langle l|\hat{V}|k\rangle \langle k|\hat{V}|m\rangle}{E_k - (E_l - E_m)/2}, \quad (2)$$

where $l, m = 1, 2$ denote the levels |1> and |2> (see Fig. 6) of the quasidoublet, and $k = 3, \dots, 9$ represent the excited

levels. The influence of the excited levels leads to the displacement of the ground doublet as a whole (Van Vleck contribution to magnetization).

The effective spin Hamiltonian for the Zeeman energy, and for the Van Vleck contribution, which accounts for the splitting of the two lowest singlets in the crystal field, is given by

$$H_{\text{eff}}^{(q)} = \Delta\sigma_{\zeta}^{(q)} - \mu_q \mathbf{H} \sigma_{\eta}^{(q)} - \frac{1}{2} \mathbf{H} \hat{\chi}_{VV}^{(q)} \mathbf{H}, \quad (3)$$

where $\sigma_{\eta}^{(q)} = \begin{pmatrix} 0 & -i \\ i & 0 \end{pmatrix}$, $\sigma_{\zeta}^{(q)} = \begin{pmatrix} 1 & 0 \\ 0 & -1 \end{pmatrix}$ are the Pauli matrices of the position q , $\mu_q \mathbf{H} = \mu_0 \mathbf{n}_q \mathbf{H} = -i\mu_B g_J \langle 1|\hat{\mathbf{J}}_q \mathbf{H}|2\rangle$, \mathbf{n}_q represents an arbitrarily oriented easy axis, \mathbf{H} denotes the external magnetic field, and $\hat{\chi}_{VV}^{(q)}$ stands for the Van Vleck local susceptibility.

The energy levels of the Pr^{3+} lowest singlets in a position q , obtained by diagonalizing the Hamiltonian in Eq. (3), are given by

$$E_q^{(\pm)}(\mathbf{H}, \Delta) = -\varepsilon_{VV} \pm \Delta_q, \quad (4)$$

where $\varepsilon_{VV} = \frac{1}{2} \mathbf{H} \hat{\chi}_{VV} \mathbf{H}$ is the displacement of the two singlets' "center of mass" due to the admixture of excited states in the field and $\Delta_q = \sqrt{(\mu_q \mathbf{H})^2 + \Delta^2}$ denotes the effective field splitting. Considering the excited levels $k = 3, \dots, 9$, described by the "center of mass" Δ_{cf2} (Fig. 6) with degeneracy $g = 7$, we introduce the statistical sum Z_q of the ion at position q ,

$$Z_q(\mathbf{H}, T, \Delta) = e^{-\frac{E_q^{(+)}(\mathbf{H}, \Delta)}{k_B T}} + e^{-\frac{E_q^{(-)}(\mathbf{H}, \Delta)}{k_B T}} + g e^{-\frac{\Delta_{cf2}}{k_B T}}, \quad (5)$$

and the free energy of the system per single magnetic ion,

$$f(\mathbf{H}, T) = -\frac{1}{6} k_B T \sum_q \int (\ln Z_q(\mathbf{H}, T, \Delta)) \rho(\Delta) d\Delta, \quad (6)$$

where k_B is the Boltzmann constant and T denotes the temperature.

Differentiating Eq. (6) with respect to the field \mathbf{H} , we obtain the magnetization:

$$\mathbf{M}(\mathbf{H}, T) \approx \frac{1}{6Z^{(0)}(T)} \sum_q \mu_q (\mu_q \mathbf{H}) \chi_q(\mathbf{H}, T) + \hat{\chi}_{VV}(T) \mathbf{H} + \hat{\chi}_{3-9}(T) \mathbf{H}, \quad (7)$$

where $Z^{(0)} = 1 + g e^{-\frac{\Delta_{cf2}}{k_B T}}/2$ reflects the change in the population of excited levels. This is determined by the magnitude of their "center of mass" $\Delta_{cf2} \approx 260 \pm 50$ K (derived from the fit of the magnetic susceptibility at high temperatures), $\hat{\chi}^{vv} = \sum_q \hat{\chi}_{VV}^{(q)}/6Z^{(0)}(T)$ with

$$\chi_q(\mathbf{H}, T) = \int \frac{1}{\Delta_q} \text{th} \left(\frac{\Delta_q}{k_B T} \right) \rho(\Delta) d\Delta \quad (8)$$

representing the effective local magnetic susceptibility of the Pr^{3+} ground quasidoublet in a position q . The integration in Eq. (8) takes into account the crystal field splitting distribution arising from the random filling of the $2d$ positions by Ga and Si. The last two terms in Eq. (7) give the Van Vleck contribution and the contribution arising from

transitions between excited states $k = 3, \dots, 9$: $\hat{\chi}_{3-9}(T) = g\widehat{\mu_{\text{eff}}^2} e^{-\frac{\Delta_{\text{eff}}}{k_B T}} / 2k_B T Z^{(0)}(T)$, respectively. The tensor $\widehat{\mu_{\text{eff}}^2}$ is determined by the squared effective matrix elements along, $(\mu_{\text{eff}}^{\parallel})^2$, and perpendicular to $(\mu_{\text{eff}}^{\perp})^2$, the c axis.

The random filling of the $2d$ positions by Ga and Si ions results in a large number of inequivalent positions and, in general, leads to a distribution of the orientations of the easy axes. We assign arbitrary orientations to the local axis of the rare-earth ion $\mathbf{n}_{1+}(\varphi, \theta) = (\cos \varphi \sin \theta, \sin \varphi \sin \theta, \cos \theta)$ (where φ and θ are azimuthal and polar angles, respectively) due to the lack of symmetry in the local environment. However, according to x-ray diffraction studies [19] and to the angular dependencies of magnetization (see Sec. III, Experiment), the global symmetry $P321$ of rare-earth langasites remains preserved. This preservation allows us to connect the nonequivalent positions of magnetic ions through symmetry operations C_2 and C_3 . The $C_2 \parallel a \parallel x$ symmetry transforms the \mathbf{n}_{1+} local axis to \mathbf{n}_{1-} , where the components are $n_{1+}^{(x)} = n_{1-}^{(x)}$, $n_{1+}^{(y)} = -n_{1-}^{(y)}$, $n_{1+}^{(z)} = -n_{1-}^{(z)}$. Additionally, the rotations by $+120^\circ$ and -120° connect the position “1 \pm ” with “2 \pm ” and “3 \pm ”, respectively ($\mathbf{n}_{2\pm,3\pm} = \hat{C}_3^\pm \mathbf{n}_{1\pm}$, where \hat{C}_3^\pm are rotation matrices). Thus, the easy axes in positions “1 \pm ”, “2 \pm ”, and “3 \pm ” restore the $P321$ symmetry, despite this symmetry being locally broken.

The absence of a saturation in the magnetization curves at fields up to 5 T at low temperatures point toward significant splitting between the two lowest singlets of the Pr^{3+} ion. Consequently, the weak influence of the easy axes’ distribution on the experimental angular dependencies of magnetization suggests that it is sufficient to use only the average directions of easy axes (i.e., without considering their distribution) to describe the magnetic and magnetoelectric properties.

Based on the above-formulated model for the Pr^{3+} energy spectrum and its magnetic structure, we performed a consistent modeling of the magnetization for different field dependencies (Fig. 2), angular dependencies (Fig. 3), and temperature dependencies (Fig. 4). This modeling enabled us to determine the magnetic moment of the Pr^{3+} quasideoublet as $\mu_0 = (2.34^\circ \pm 0.07^\circ) \mu_B$ and the local easy axis orientation $\bar{\varphi} = -90^\circ \pm 1^\circ$ and $\bar{\theta} = 45.5^\circ \pm 1.0^\circ$ (in the “1+” position). Since the averaged easy axes lie in the b^*c plane, \mathbf{n}_{q+} and \mathbf{n}_{q-} are equivalent (Fig. 7); we denote them as \mathbf{n}_q henceforth.

The theoretical angular dependence of magnetization in the b^*c plane exhibits a pronounced asymmetry with respect to the b^* axis. The first feature arises at 44.5° from the c axis, when the field is orthogonal to \mathbf{n}_1 . The minimum of the angular dependence occurs when the magnetic field approaches the direction orthogonal to the axes $\mathbf{n}_{2,3}$. The small difference between experimental and theoretical curves in angular dependencies in the b^*c plane [Fig. 3(c)] could be associated with neglect of the easy axes’ distribution within the simplified model. The distribution of the anisotropy axes’ orientations may lead to the smoothing out of the angular dependencies and to a reduction of its asymmetry with respect to the b^* axes. We cannot exclude that such a distribution could be observed in higher magnetic fields or in local susceptibility measurements by polarized neutron scattering.

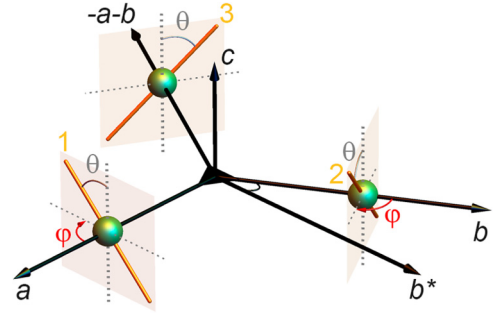


FIG. 7. Schematic representation of the Pr^{3+} easy axis directions in PGS. The axes in local positions are oriented at angles $\bar{\varphi} = -90^\circ \pm 1^\circ$ (in the b^*c plane and equivalent planes) and $\bar{\theta} = 45.5^\circ \pm 1.0^\circ$ (average azimuthal and polar angles). The C_2 and C_3 symmetry operations connect the magnetization axes, which restores the global $P321$ symmetry.

C. Temperature dependence of magnetic susceptibility

We performed simulations of the magnetic susceptibility of PGS over a wide temperature range and determined the parameter σ , which characterizes the crystal field splitting distribution resulting from the local symmetry breaking.

The expansion of the effective local susceptibility, Eq. (8), with respect to a weak magnetic field $(\mu_q \mathbf{H}) \ll k_B T$, Δ takes the form:

$$\begin{aligned} \chi_q(\mathbf{H}, T) = & \int \frac{1}{\Delta} th\left(\frac{\Delta}{k_B T}\right) \rho(\Delta) d\Delta \\ & + \int \frac{1}{2\Delta} \left[\frac{\Delta}{k_B T} \cosh^{-2}\left(\frac{\Delta}{k_B T}\right) \right. \\ & \left. - th\left(\frac{\Delta}{k_B T}\right) \right] \left(\frac{\mu_q \mathbf{H}}{\Delta}\right)^2 \rho(\Delta) d\Delta. \end{aligned} \quad (9)$$

The first term is independent of the magnetic field and it determines the contribution from the two lowest singlets to the temperature dependence of the magnetic susceptibilities and the polarization in the ab^* plane (see below). The second term depends on the orientation of the local easy axis with respect to the magnetic field. At high temperatures, it is proportional to $\sim T^{-3}$ and it determines the magnetoelectric susceptibility along the c axis (see below).

Below 50 K, only the two lowest singlets determine the temperature behavior of the magnetic susceptibility. Using the expansion from Eq. (9) for the magnetization described in Eq. (7), one can isolate the main contribution to the total magnetic susceptibility along applied field in this temperature region:

$$\begin{aligned} \chi_H(T) = & \left. \frac{dM(\mathbf{H}, T)}{dH} \right|_{H \rightarrow 0} \\ = & \frac{1}{6} \sum_q \frac{(\mu_q \mathbf{H})^2}{H^2} \int \frac{1}{\Delta} th\left(\frac{\Delta}{k_B T}\right) \rho(\Delta) d\Delta + \hat{\chi}_{\text{vv}}. \end{aligned} \quad (10)$$

The temperature dependence of the derivative $d\chi_H(T)/dT = -\sum_q \int (\mu_q \mathbf{H})^2 \rho(\Delta) d\Delta / 6H^2 k_B T^2 \cosh^2 \Delta / k_B T$ has only one free parameter σ and it is determined by the

TABLE I. The list of values of magnetic and magnetoelectric model parameters with their errors. The magnetic parameters are σ , parameter of distribution function [Eq. (1)] with mean value $\bar{\Delta}_{cf}$; μ_0 , magnetic moment of the Pr^{3+} quasidoublet; $\bar{\varphi}$ and $\bar{\theta}$, azimuthal and polar angles of the local easy axis in the “1+” position; χ_{VVa} , χ_{VVb} , and χ_{VVc} , the Van Vleck susceptibilities; Δ_{cf2} , the “center of mass” of excited levels; $\mu_{\text{eff}}^{\parallel} \approx \mu_{\text{eff}}^{\perp}$, effective magnetic moment of excited levels; L_i , magnetoelectric phenomenological constants; and $\alpha_{1/2}^{VV}$, magnetoelectric Van Vleck contributions. Braces define the temperature range where the magnetic parameters are significant.

	Parameters	Value	
Magnetic	σ	11.5 ± 1.0 K	$\left. \begin{array}{l} T > 50 \text{ K} \\ \\ T > 50 \text{ K} \end{array} \right\}$
	$\bar{\Delta}_{cf}$	14.4 ± 1.4 K	
	μ_0	$18(3)$ K [26]	
	$\bar{\varphi}$	20 K [36]	
	$\bar{\theta}$	$(2.34 \pm 0.07) \mu_B$	
	$\chi_{VVa}, = \chi_{VVb}$	$-90^\circ \pm 1^\circ$	
	χ_{VVc}	$45.5^\circ \pm 1.0^\circ$	
	Δ_{cf2}	$(2.4 \pm 0.5) \times 10^{-5} \text{ cm}^3/\text{g}$	
	$\mu_{\text{eff}}^{\parallel} = \mu_{\text{eff}}^{\perp}$	$(1.7 \pm 0.3) \times 10^{-5} \text{ cm}^3/\text{g}$	
		260 ± 50 K	
Magnetoelectric		$(0.7 \pm 0.1) \mu_B$	
	L_1	$38 \pm 1 \mu\text{C}/(\text{m}^2 \text{T})$	
	L_2	$14 \pm 1 \mu\text{C}/(\text{m}^2 \text{T})$	
	L_3	$123 \pm 1 \mu\text{C}/(\text{m}^2 \text{T})$	
	L_4	$-7 \pm 1 \mu\text{C}/(\text{m}^2 \text{T})$	
	α_1^{VV}	$0.14 \pm 0.02 \mu\text{C}/(\text{m}^2 \text{T}^2)$	
	α_2^{VV}	$0.19 \pm 0.02 \mu\text{C}/(\text{m}^2 \text{T}^2)$	

two lowest singlets. Here, the Van Vleck contribution does not depend on temperature. For $H \parallel c$, the sum over projections of the magnetic moments onto the field is $\sum_q (\boldsymbol{\mu}_q \mathbf{H})^2 / H^2 \approx 3\mu_z^2$. For $H \parallel a$, it equals $\sum_q (\boldsymbol{\mu}_q \mathbf{H})^2 / H^2 \approx 1.5\mu_y^2$. The ratio of two terms is equal to $\cos^2 \bar{\theta} / \sin^2 \bar{\theta} \approx 1.97$ (where $\bar{\theta}$ is determined from the angular dependencies) and serves as the proportionality coefficient between the temperature dependencies of the magnetic susceptibilities' derivatives (inset in Fig. 4). The behavior of both is identical and is well described by $\sigma = 11.5 \pm 1.1$ K, in the distribution $\rho(\Delta)$, which corresponds to the variance $D_{\bar{\Delta}} = \sigma \sqrt{2 - \pi} / 2 = 7.5 \pm 0.7$ K. The mean value $\bar{\Delta}_{cf} = \sigma \sqrt{\pi} / 2 = 14.4 \pm 1.4$ K indicates an average energy splitting between the two lowest singlets, which is in good agreement with 18(3) K and 20 K observed by muon spin relaxation [26] and by specific-heat [36] experiments, respectively.

At higher temperatures ($T > 50$ K), the contributions from the Van Vleck term and from the transitions between excited levels of Pr^{3+} ($k = 3, \dots, 9$) significantly contribute to the temperature dependence of χ . As the temperature increases, the population of the two lowest singlets decreases, leading to a decrease in χ_{VV} (Fig. 4). The refined Van Vleck susceptibilities are equal to $\chi_{VVa} = (2.4 \pm 0.5) \times 10^{-5} \text{ cm}^3/\text{g}$ and $\chi_{VVc} = (1.7 \pm 0.3) \times 10^{-5} \text{ cm}^3/\text{g}$ for the field in the basal plane and perpendicular to it, respectively. From this, the effective contributions to the magnetic moment are obtained as $\mu_{\text{eff}}^{a,b^*} = (1.7 \pm 0.3) \mu_B$ and $\mu_{\text{eff}}^c = (1.4 \pm 0.3) \mu_B$ (Table I).

At high temperatures, $T > 120$ K, the transitions within the excited levels make the notable nonmonotonic contribution to the magnetic susceptibility, which we effectively account for in Eq. (7) (Fig. 4). An estimate of the effective

magnetic moment of excited levels is

$$\mu_{\text{eff}}^{\parallel} \approx \mu_{\text{eff}}^{\perp} = (0.7 \pm 0.1) \mu_B.$$

In general, the local symmetry breaking, that leads to a distribution of the crystal field splitting, influences not only the magnetic properties but also the electric polarization.

D. Polarization

We consider the influence of both magnetic \mathbf{H} and electric \mathbf{E} fields [28] on Pr^{3+} ions to describe the magnetoelectric properties of PGS. In this case, the expression $\hat{V} = -\hat{\mathbf{d}}\mathbf{E} + \mu_{BGL}\hat{\mathbf{J}}\mathbf{H}$ describes the perturbation operator \hat{V} , where the first term is the interaction of the effective dipole moment $\hat{\mathbf{d}}$ with the electric field and the second term represents the Zeeman interaction, mentioned earlier. As previously shown in Eq. (2), we construct the second-order perturbation theory matrix of the total energy in the space of the two lowest states of Pr^{3+} and determine the magnetoelectric part of the spin Hamiltonian of the q th position in the local coordinate system (denoted by a prime):

$$H'_{\text{ME}}{}^{(q)} = -\mathbf{E}'_q \hat{\mathbf{g}}_{\text{ME}} \mathbf{H}'_q \sigma_{\eta}. \quad (11)$$

At arbitrary local symmetry (C_1), the tensor of microscopic (local) magnetoelectric interactions $\hat{\mathbf{g}}_{\text{ME}}$ has all nine components.

Using the magnetoelectric part of the spin Hamiltonian, Eq. (11), and the definition of the magnetic moment of the quasidoublet $\boldsymbol{\mu}' \mathbf{H}'_q = \mu_0 \mathbf{n}' \mathbf{H}'_q = -i \mu_{BGL} \langle A | \hat{\mathbf{J}} \mathbf{H}'_q | B \rangle$, we obtain the magnetoelectric contribution to the splitting $\Delta'_q = \sqrt{(\boldsymbol{\mu}' \mathbf{H}'_q + \mathbf{E}'_q \hat{\mathbf{g}}_{\text{ME}} \mathbf{H}'_q)^2} + \Delta^2$. Here the local coordinate system is chosen such that $\mathbf{n}' = (1, 0, 0)$. In this case,

TABLE II. Irreducible representations of the $P321$ space group and transformation properties of the magnetic field \mathbf{H} components, nonlinear susceptibilities χ , χ_{123} , and χ_{23} , and electric field \mathbf{E} .

Representation	Matrices of the representations of the group			\mathbf{H} components		Magnetic susceptibility	Irreducible combinations	\mathbf{E}
	E	C_2	2_a	H_c	H_c^2	$\chi(H)$	of χ and \mathbf{H} components	
Γ_1	1	1	1		$H_a^2 + H_{b^*}^2; H_c^2$	χ		
Γ_2	1	1	-1	H_c			$\chi_{23}H_{b^*}H_c - \chi_{123}(-H_aH_c)$	E_c
Γ_3	1	$\begin{pmatrix} -1/2 & -\sqrt{3}/2 \\ \sqrt{3}/2 & -1/2 \end{pmatrix}$	$\begin{pmatrix} 1 & 0 \\ 0 & -1 \end{pmatrix}$	$\begin{pmatrix} H_a \\ H_{b^*} \end{pmatrix}$	$\begin{pmatrix} H_{b^*}H_c \\ -H_aH_c \end{pmatrix}$	$\begin{pmatrix} H_a^2 - H_{b^*}^2 \\ -2H_aH_{b^*} \end{pmatrix}$	$\begin{pmatrix} \chi_{123} \\ \chi_{23} \end{pmatrix}$	$\chi \begin{pmatrix} H_{b^*}H_c \\ (-H_aH_c) \end{pmatrix}; \chi \begin{pmatrix} H_a^2 - H_{b^*}^2 \\ (-2H_aH_{b^*}) \end{pmatrix}; \begin{pmatrix} E_a \\ E_{b^*} \end{pmatrix}$

the free energy of the q th position is given by $f'_q = -\frac{1}{6}k_B T \int \ln(2 \cosh \Delta') \rho(\Delta) d\Delta$ and the local electric polarization is obtained by

$$\mathbf{P}'_q = -\partial f'_q / \partial \mathbf{E}'_q = \hat{g}_{\text{ME}} \mu_0 \mathbf{H}'_q (\mathbf{n}' \mathbf{H}'_q) \chi_q, \quad (12)$$

where χ_q is the effective local magnetic susceptibility, Eq. (8). Here, we omitted the contribution from the excited states in the statistical sum. As a result, the superposition of the local electric polarizations \mathbf{P}'_q from nonequivalent positions, transformed into the crystallographic coordinate system by the transformation matrix \hat{S}'_q , forms the macroscopic polarization $\mathbf{P} = \sum_q \hat{S}'_q \mathbf{P}'_q = \sum_q \mathbf{P}_q$.

The symmetry operations C_2 and C_3 connect the nonequivalent local positions of Pr^{3+} , establishing correlations between local magnetic susceptibilities, Eq. (8). For example, a C_2 symmetry operation relates χ_{1+} and χ_{1-} . Therefore, their sum is invariant with respect to C_2 , while their difference changes sign. Similarly, C_3 connects $\chi_{2\pm}$ and $\chi_{3\pm}$ with $\chi_{1\pm}$; their combinations may belong to different representations of the space group. However, as we concluded from the analysis of the magnetic properties, it is sufficient to use average directions of the local anisotropy axes, which lie in the b^*c plane and satisfy the C_2 symmetry ($\chi_{q+} = \chi_{q-}$). This allows us to reduce the number of irreducible combinations of the effective local magnetic susceptibilities to three:

$$\begin{aligned} \chi &= \frac{1}{3}(\chi_1 + \chi_2 + \chi_3), & \chi_{123} &= \frac{1}{3}(2\chi_1 - \chi_2 - \chi_3), \\ \chi_{23} &= \frac{\sqrt{3}}{3}(\chi_2 - \chi_3). \end{aligned} \quad (13)$$

The total magnetic susceptibility χ reflects the collective response of the magnetic subsystem. It is finite for $H \rightarrow 0$ and decreases with increasing field due to the saturation of magnetic moments. On the other hand, the combinations χ_{123} and χ_{23} equal zero for $H \rightarrow 0$. As the field strength increases, various positions will react in different ways, leading to deviation of χ_{123} and χ_{23} from zero. This process continues until the moments reach saturation.

Table II presents the transformation properties of irreducible combinations χ , χ_{123} , and χ_{23} , and the magnetic and electric fields. We derive the relevant combinations of susceptibilities and the components of the magnetic field belonging to the same representations as the electric field \mathbf{E} . We note that there is no saturation of magnetic moments up to 5 T. Therefore, the microscopic features of the polarization

do not become relevant, and a phenomenological approach with a limited number of magnetoelectric terms remains sufficient. More specifically, the symmetrized combinations of the effective local magnetic susceptibilities, Eq. (13), with quadratic combinations of the magnetic field components, define the electric polarization. Thus, the field dependence of the in-plane components P_{a,b^*} and the out-of-plane component P_c is solely described by two phenomenological constants, $L_{1,2}$ and $L_{3,4}$.

The magnetoelectric part of the thermodynamic potential $\Phi_{\text{ME}}(H, T)$, obtained by combining the electric field in the ab^* plane (E_{a,b^*}) with irreducible combinations of local effective susceptibilities and magnetic field components belonging to Γ_3 , is given by

$$\begin{aligned} \Phi_{\text{ME}}(H, T) &= -\frac{L_1 \mu_0}{Z^{(0)}(T)} (E_a H_{b^*} H_c - E_{b^*} H_a H_c) \chi(\mathbf{H}, T) \\ &\quad - \frac{L_2 \mu_0}{Z^{(0)}(T)} (E_a (H_a^2 - H_{b^*}^2) - 2E_{b^*} H_a H_{b^*}) \chi(\mathbf{H}, T) \\ &\quad - \frac{\alpha_1^{\text{vV}}}{Z^{(0)}(T)} (E_a H_{b^*} H_c - P_{b^*} H_a H_c) \\ &\quad - \frac{\alpha_2^{\text{vV}}}{Z^{(0)}(T)} (E_a (H_a^2 - H_{b^*}^2) - 2E_{b^*} H_a H_{b^*}) + \dots \quad (14) \end{aligned}$$

Here we consider the symmetry-allowed Van Vleck contribution, as well as the temperature dependence of the statistical sum $Z^{(0)}$ due to increasing population of the excited states.

The combinations of χ_{123} and χ_{23} with quadratic components of the magnetic field [such as $E_a(\chi_{123}H_{b^*}H_c - \chi_{23}(-H_aH_c)) + E_{b^*}(-\chi_{123}(-H_aH_c) - \chi_{23}H_{b^*}H_c)$] also belong to the Γ_3 representation. However, their lowest order is H^4 , indicating that these components only weakly influence the planar polarization in the parameter range of interest.

As a result, the a and b^* components of the polarizations are given by

$$\begin{aligned} P_a(H, T) &= \alpha_1(\mathbf{H}, T) H_{b^*} H_c + \alpha_2(\mathbf{H}, T) (H_a^2 - H_{b^*}^2), \\ P_{b^*}(H, T) &= \alpha_1(\mathbf{H}, T) (-H_a H_c) + \alpha_2(\mathbf{H}, T) (-2H_a H_{b^*}), \end{aligned} \quad (15)$$

where $\alpha_{1,2}(\mathbf{H}, T) = (L_{1,2} \mu_0 \chi(\mathbf{H}, T) + \alpha_{1,2}^{\text{vV}}) / Z^{(0)}(T)$ are the quadratic magnetoelectric susceptibilities. Considering the connection between the local polarization of the q th position and the macroscopic polarization $\mathbf{P} = \sum_q \hat{S}'_q \mathbf{P}'_q$, the compo-

nents of the microscopic tensor \hat{g}_{ME} , Eq. (12), define the phenomenological constants $L_{1,2}$.

Using the expressions above, we carried out modeling of the field dependencies of P_a at various temperatures (Fig. 5). For $T < 50$ K and $H \rightarrow 0$, the main contribution to the magnetoelectric susceptibilities, $\alpha_{1,2}(T) = L_{1,2}\mu_0\chi(T) + \alpha_{1,2}^{\text{VV}}$, comes from the temperature-dependent effective local magnetic susceptibility, Eq. (8) [Fig. 5(c)] with parameters μ_0 , $\bar{\varphi}$, $\bar{\theta}$, and σ received from the magnetic data (Table I). For higher temperatures, the Van Vleck contribution is important and $Z^{(0)}(T)$ have to be taken into account in $\alpha_{1,2}(\mathbf{H}, T)$. Thus, phenomenological constants $L_{1,2}$ and $\alpha_{1,2}^{\text{VV}}$ (Table I) are obtained from consistent modeling of P_a .

It is worth mentioning that, throughout the entire range of temperatures and magnetic fields, the relationships $P_a(H_a) = -P_a(H_{b^*})$ and $P_a(H_{a45b^*45^\circ c}) = -P_a(H_{a45b^*135^\circ c})$ hold, which follows from Eq. (15) and the expansion of χ .

At low temperatures and in strong magnetic fields up to 5 T, slight deviations between theoretical predictions and experimental observations are seen. In this regime, additional contributions to the polarization coming from χ_{123} and χ_{23} become relevant. These contributions arise from the nonequivalence of different positions under an external magnetic field, resulting in a correction to the in-plane polarization (P_{a,b^*}). On the contrary, in the P_c component, these effects become apparent even at fields below 5 T.

The polarization along the trigonal axis, P_c , transforms according to the one-dimensional representation Γ_2 of the $P321$ group. This representation incorporates combinations starting from the fourth power of the field $H_x H_z (H_x^2 - 3H_y^2)$ and does not include quadratic terms. In our case, the quadratic combinations of magnetic field components with susceptibilities χ_{123} and χ_{23} determine the polarization P_c , which can be represented as follows (see Table II):

$$P_c(H, T) = L_3\mu_0(\chi_{23}H_{b^*}H_c - \chi_{123}(-H_aH_c)) \\ + L_4\mu_0(\chi_{23}(H_a^2 - H_{b^*}^2) - \chi_{123}(-2H_aH_{b^*})). \quad (16)$$

In the regime of small fields and high temperatures, $\mu_q H \ll k_B T$, Δ , only one phenomenological constant determines the polarization $P_c \sim H^4$:

$$P_c(H, T) = -\alpha^{(4)}(T)H_aH_c(H_a^2 - 3H_{b^*}^2), \\ \alpha^{(4)}(T) = \left[\frac{1}{2}L_3n_y^2 + 2L_4n_y n_z \right] \\ \times \int \frac{\mu_0^3}{2\Delta^3} \left[\frac{\Delta}{k_B T} \cosh^{-2}\left(\frac{\Delta}{k_B T}\right) - \text{th}\left(\frac{\Delta}{k_B T}\right) \right] \\ \times \rho(\Delta)d\Delta, \quad (17)$$

where the expansion, Eq. (9), for effective local susceptibilities was used in symmetrized combinations, Eq. (13), along with the definition $\mathbf{n}(\bar{\theta}) = (0, n_y, n_z) = (0, \sin\bar{\theta}, \cos\bar{\theta})$. The estimation of the phenomenological constant is $\frac{1}{2}L_3n_y^2 + 2L_4n_y n_z \approx 24 \mu\text{C}/(\text{m}^2 \text{T})$. The integrand determines the temperature dependence of the magnetoelectric susceptibility $\alpha^{(4)}(T)$ [see inset in Fig. 5(d)]. At temperatures $T > 15$ K the $\alpha^{(4)}(T)$ is proportional to T^{-3} . However, at low temperatures the distribution of the crystal field splitting becomes crucial,

which leads to a slightly slower temperature dependence for $\alpha^{(4)}(T)$. This is similar to the behavior of the magnetic, Eq. (10), and quadratic magnetoelectric, $\alpha_{1,2}$, susceptibilities.

In magnetic fields around 5 T and at low temperatures ($T < 5$ K), the polarization shows a tendency for linear behavior [Fig. 5(d)], and the quadratic expansion of the magnetic susceptibilities is insufficient to describe P_c . The field dependencies of the susceptibilities χ_{123} and χ_{23} are calculated in Eq. (16), and, taking into account the value of $\frac{1}{2}L_3n_y^2 + 2L_4n_y n_z$, we obtain the phenomenological constants as $L_3 = 123 \pm 1 \mu\text{C}/(\text{m}^2 \text{T})$ and $L_4 = -7 \pm 1 \mu\text{C}/(\text{m}^2 \text{T})$ (Table I).

As mentioned above, the phenomenological constants L_i are determined by combinations of microscopic parameters with components of the local magnetization in a distorted local environment. Due to the large value of $\bar{\Delta}_{cf}$, the microscopic features associated with strong anisotropy of the Pr^{3+} ion are weak up to fields of 5 T. To describe them quantitatively and to establish the relationship between the phenomenological constants and the microscopic parameters, measurements of electric polarization in stronger magnetic fields are necessary.

V. CONCLUSION

Here we present a comprehensive experimental and theoretical investigation of magnetic and magnetoelectric properties of Pr^{3+} -doped langasite. We observe the magnetic-field-induced electric polarization in this material and provide an explanation for this phenomenon.

Our experimental efforts involved detailed measurements of magnetization along the principal crystallographic axes, angular dependencies in various planes, and magnetic susceptibility. Notably, we found that the component of induced polarization in the basal ab^* plane (P_a) exhibits a quadratic dependence on the magnetic field, while the polarization along the trigonal axis (P_c) shows only the fourth power of the field (H^4), with a tendency to become quasilinear in fields close to 5 T.

To give insight to these phenomena, we suggest a model assuming a quasidoublet ground state of the Pr^{3+} ion in the crystal field. The random occupation of the $2d$ positions by Ga and Si ions in PGS leads to a breaking of the local C_2 symmetry, resulting in a distribution of the quasidoublet splitting and of the orientations of the local anisotropy axes. However, the C_2 symmetry and the rotation around the trigonal c axis connects these local axes in different crystallographic positions, thus restoring the global $P321$ symmetry of the crystal.

From fitting of the experimental data, we demonstrated that the average anisotropy axes of Pr^{3+} lie in the b^*c plane, while the behavior of magnetic susceptibility at low temperatures is strongly influenced by the distribution of the crystal field splitting.

Furthermore, we developed a phenomenological approach to describe the field-induced electric polarization, demonstrating that the polarization in local positions depends on effective local magnetic susceptibilities. The macroscopic polarization is determined by a superposition of these local contributions. In particular, irreducible combinations of local

effective susceptibilities allow us to take into account both the global symmetry and the specific features of the Pr^{3+} ground state.

The sensitivity of the temperature dependence of magnetic and magnetoelectric susceptibilities allowed us to estimate the average magnitude and dispersion to the crystal field distribution. Our findings have implications beyond PGS langasite, suggesting that the influence of local distortions on the ground state and on magnetic and magnetoelectric properties may also manifest itself in other langasite materials doped with different rare-earth ions.

This work unveils the intricate interplay between crystal structure, local symmetry, and magnetoelectric properties in langasites, paving the way for further investigations.

ACKNOWLEDGMENTS

This work was supported by the Russian Science Foundation (Project No. 22–42–05004) and by the Austrian Science Funds (Projects No. P32404 and No. I5539).

-
- [1] G. T. Rado and V. J. Folen, Observation of the magnetically induced magnetoelectric effect and evidence for antiferromagnetic domains, *Phys. Rev. Lett.* **7**, 310 (1961).
- [2] M. Fiebig, Revival of the magnetoelectric effect, *J. Phys. D: Appl. Phys.* **38**, R123 (2005).
- [3] M. M. Vopson, Fundamentals of multiferroic materials and their possible applications, *Crit. Rev. Solid State Mater. Sci.* **40**, 223 (2015).
- [4] S. Manipatruni, D. E. Nikonov, and I. A. Young, Beyond CMOS computing with spin and polarization, *Nat. Phys.* **14**, 338 (2018).
- [5] W. Kleemann, Magnetoelectric spintronics, *J. Appl. Phys.* **114**, 1 (2013).
- [6] F. Matsukura, Y. Tokura, and H. Ohno, Control of magnetism by electric fields, *Nat. Nanotechnol.* **10**, 209 (2015).
- [7] W. Eerenstein, N. D. Mathur, and J. F. Scott, Multiferroic and magnetoelectric materials, *Nature (London)* **442**, 759 (2006).
- [8] R. Gupta and R. K. Kotnala, A review on current status and mechanisms of room-temperature magnetoelectric coupling in multiferroics for device applications, *J. Mater. Sci.* **57**, 12710 (2022).
- [9] N. A. Hill, Why are there so few magnetic ferroelectrics?, *J. Phys. Chem. B* **104**, 6694 (2000).
- [10] T. Kimura, T. Goto, H. Shintani, K. Ishizaka, T. Arima, and Y. Tokura, Magnetic control of ferroelectric polarization, *Nature (London)* **426**, 55 (2003).
- [11] Y. Tokura, S. Seki, and N. Nagaosa, Multiferroics of spin origin, *Rep. Prog. Phys.* **77**, 76501 (2014).
- [12] N. A. Spaldin and R. Ramesh, Advances in magnetoelectric multiferroics, *Nat. Mater.* **18**, 203 (2019).
- [13] S. Picozzi and C. Ederer, First principles studies of multiferroic materials, *J. Phys. Condens. Matter* **21**, 303201 (2009).
- [14] K. Marty, P. Bordet, V. Simonet, M. Loire, R. Ballou, C. Darie, J. Kljun, P. Bonville, O. Isnard, P. Lejay, B. Zawilski, and C. Simon, Magnetic and dielectric properties in the langasite-type compounds: $A_3B\text{Fe}_3D_2\text{O}_{14}$ ($A = \text{Ba, Sr, Ca}$; $B = \text{Ta, Nb, Sb}$; $D = \text{Ge, Si}$), *Phys. Rev. B* **81**, 054416 (2010).
- [15] K. Marty, V. Simonet, E. Ressouche, R. Ballou, P. Lejay, and P. Bordet, Single domain magnetic helicity and triangular chirality in structurally enantiopure $\text{Ba}_3\text{NbFe}_3\text{Si}_2\text{O}_{14}$, *Phys. Rev. Lett.* **101**, 247201 (2008).
- [16] H. D. Zhou, L. L. Lumata, P. L. Kuhns, A. P. Reyes, E. S. Choi, N. S. Dalal, J. Lu, Y. J. Jo, L. Balicas, J. S. Brooks, and C. R. Wiebe, $\text{Ba}_3\text{NbFe}_3\text{Si}_2\text{O}_{14}$: A new multiferroic with a 2D triangular Fe^{3+} motif, *Chem. Mater.* **21**, 156 (2009).
- [17] N. Lee, Y. J. Choi, and S. W. Cheong, Magnetic control of ferroelectric polarization in a self-formed single magnetoelectric domain of multiferroic $\text{Ba}_3\text{NbFe}_3\text{Si}_2\text{O}_{14}$, *Appl. Phys. Lett.* **104**, 072904 (2014).
- [18] H. Narita, Y. Tokunaga, A. Kikkawa, Y. Taguchi, Y. Tokura, and Y. Takahashi, Observation of nonreciprocal directional dichroism via electromagnon resonance in a chiral-lattice helimagnet $\text{Ba}_3\text{NbFe}_3\text{Si}_2\text{O}_{14}$, *Phys. Rev. B* **94**, 094433 (2016).
- [19] P. Bordet, I. Gelard, K. Marty, A. Ibanez, J. Robert, V. Simonet, B. Canals, R. Ballou, and P. Lejay, Magnetic frustration on a kagomé lattice in $\text{R}_3\text{Ga}_5\text{SiO}_{14}$ langasites with $\text{R} = \text{Nd, Pr}$, *J. Phys. Condens. Matter* **18**, 5147 (2006).
- [20] A. Y. Tikhonovskii, V. Y. Ivanov, A. M. Kuzmenko, A. M. Balbashov, Z. Wang, V. Skumryev, and A. A. Mukhin, Magnetoelectric phenomena in Fe langasites, *Phys. Rev. B* **105**, 104424 (2022).
- [21] H. D. Zhou, B. W. Vogt, J. A. Janik, Y. J. Jo, L. Balicas, Y. Qiu, J. R. D. Copley, J. S. Gardner, and C. R. Wiebe, Partial field-induced magnetic order in the spin-liquid kagomé $\text{Nd}_3\text{Ga}_5\text{SiO}_{14}$, *Phys. Rev. Lett.* **99**, 236401 (2007).
- [22] A. Zorko, F. Bert, P. Mendels, P. Bordet, P. Lejay, and J. Robert, Easy-axis kagome antiferromagnet: Local-probe study of $\text{Nd}_3\text{Ga}_5\text{SiO}_{14}$, *Phys. Rev. Lett.* **100**, 147201 (2008).
- [23] V. Simonet, R. Ballou, J. Robert, B. Canals, F. Hippert, P. Bordet, P. Lejay, P. Fouquet, J. Ollivier, and D. Braithwaite, Hidden magnetic frustration by quantum relaxation in anisotropic Nd langasite, *Phys. Rev. Lett.* **100**, 237204 (2008).
- [24] J. Robert, V. Simonet, B. Canals, R. Ballou, P. Bordet, P. Lejay, and A. Stunault, Spin-liquid correlations in the Nd-langasite anisotropic kagomé antiferromagnet, *Phys. Rev. Lett.* **96**, 197205 (2006).
- [25] H. D. Zhou, C. R. Wiebe, Y.-J. Jo, L. Balicas, R. R. Urbano, L. L. Lumata, J. S. Brooks, P. L. Kuhns, A. P. Reyes, Y. Qiu, J. R. D. Copley, and J. S. Gardner, Chemical pressure induced spin freezing phase transition in kagome Pr langasites, *Phys. Rev. Lett.* **102**, 067203 (2009).
- [26] A. Zorko, F. Bert, P. Mendels, K. Marty, and P. Bordet, Ground state of the easy-axis rare-earth kagome langasite $\text{Pr}_3\text{Ga}_5\text{SiO}_{14}$, *Phys. Rev. Lett.* **104**, 057202 (2010).
- [27] A. A. Mukhin, V. Yu. Ivanov, and B. V. Mill, Observation of the magnetic field induced ferroelectricity in rare-earth langasites: $\text{Nd}_3\text{Ga}_5\text{SiO}_{14}$, in *Book of Abstracts, Moscow International Symposium on Magnetism* (Faculty of Physics, Moscow, 2017), p. 663.

- [28] L. Weymann, L. Bergen, T. Kain, A. Pimenov, A. Shuvaev, E. Constable, D. Szaller, B. V. Mill, A. M. Kuzmenko, V. Y. Ivanov, N. V. Kostyuchenko, A. I. Popov, A. K. Zvezdin, A. Pimenov, A. A. Mukhin, and M. Mostovoy, Unusual magnetoelectric effect in paramagnetic rare-earth langasite, *npj Quantum Mater.* **5**, 61 (2020).
- [29] A. K. Zvezdin, S. S. Krotov, A. M. Kadomtseva, G. P. Vorob'ev, Y. F. Popov, A. P. Pyatakov, L. N. Bezmaternykh, and E. A. Popova, Magnetoelectric effects in gadolinium iron borate $\text{GdFe}_3(\text{BO}_3)_4$, *J. Exp. Theor. Phys. Lett.* **81**, 272 (2005).
- [30] F. Yen, B. Lorenz, Y. Y. Sun, C. W. Chu, L. N. Bezmaternykh, and A. N. Vasiliev, Magnetic field effect and dielectric anomalies at the spin reorientation phase transition of $\text{GdFe}_3(\text{BO}_3)_4$, *Phys. Rev. B* **73**, 054435 (2006).
- [31] A. K. Zvezdin, G. P. Vorob'ev, A. M. Kadomtseva, Y. F. Popov, A. P. Pyatakov, L. N. Bezmaternykh, A. V. Kuvardin, and E. A. Popova, Magnetoelectric and magnetoelastic interactions in $\text{NdFe}_3(\text{BO}_3)_4$ multiferroics, *JETP Lett.* **83**, 509 (2006).
- [32] A. M. Kuz'menko, A. A. Mukhin, V. Y. Ivanov, A. M. Kadomtseva, S. P. Lebedev, and L. N. Bezmaternykh, Antiferromagnetic resonance and dielectric properties of rare-earth ferrobates in the submillimeter frequency range, *J. Exp. Theor. Phys.* **113**, 113 (2011).
- [33] K. C. Liang, R. P. Chaudhury, B. Lorenz, Y. Y. Sun, L. N. Bezmaternykh, V. L. Temerov, and C. W. Chu, Giant magnetoelectric effect in $\text{HoAl}_3(\text{BO}_3)_4$, *Phys. Rev. B* **83**, 180417(R) (2011).
- [34] A. M. Kadomtseva, Yu. F. Popov, G. P. Vorob'ev, A. P. Pyatakov, S. S. Krotov, K. I. Kamilov, V. Yu. Ivanov, A. A. Mukhin, A. K. Zvezdin, A. M. Kuz'menko, L. N. Bezmaternykh, I. A. Gudim, and V. L. Temerov, Magnetoelectric and magnetoelastic properties of rare-earth ferrobates, *Low Temp. Phys.* **36**, 511 (2010).
- [35] V. Y. Ivanov, A. M. Kuzmenko, and A. A. Mukhin, Magnetoelectric effect in ytterbium aluminum borate $\text{YbAl}_3(\text{BO}_3)_4$, *JETP Lett.* **105**, 435 (2017).
- [36] L. L. Lumata, T. Besara, P. L. Kuhns, A. P. Reyes, H. D. Zhou, C. R. Wiebe, L. Balicas, Y. J. Jo, J. S. Brooks, Y. Takano, M. J. Case, Y. Qiu, J. R. D. Copley, J. S. Gardner, K. Y. Choi, N. S. Dalal, and M. J. R. Hoch, Low-temperature spin dynamics in the kagome system $\text{Pr}_3\text{Ga}_5\text{SiO}_{14}$, *Phys. Rev. B* **81**, 224416 (2010).
- [37] A. P. Dudka, New multicell model for describing the atomic structure of $\text{La}_3\text{Ga}_5\text{SiO}_{14}$ piezoelectric crystal: Unit cells of different compositions in the same single crystal, *Crystallogr. Reports* **62**, 195 (2017).
- [38] Y. Yoneda, H. Takeda, T. Shiosaki, and J. Mizuki, Difference between local and average structures of $\text{La}_3\text{Ga}_5\text{SiO}_{14}$ crystal, *Jpn. J. Appl. Phys.* **46**, 7163 (2007).
- [39] A. M. Balbashov and S. K. Egorov, Apparatus for growth of single crystals of oxide compounds by floating zone melting with radiation heating, *J. Cryst. Growth* **52**, 498 (1981).